27th AIAA Applied Aerodynamics Conference
22 - 25 June 2009, San Antonio, Texas

AIAA 2009-4100

Modeling of Pitching and Plunging Airfoils at Reynolds Number between 1×10^4 and 6×10^4

Chang-kwon Kang[1]*, Hikaru Aono[2]*, Pat Trizila[1]*, Yeon Baik[1]*, Jonathan M. Rausch[1]*, Luis Bernal[3]*, Michael V. Ol[4]**, and Wei Shyy[5]*

University of Michigan, Ann Arbor, MI 48109, U.S.A.

***U.S. Air Force Research Laboratory, Wright-Patterson Air Force Base, OH 45433, U.S.A.*

Fluid physics associated with a pitching and plunging airfoil, while critical to the development of flapping wing air vehicles, is not adequately understood. To help assess the state-of-the-art of engineering predictive tools, we utilize recently obtained experimental information based on particle image velocimetry (PIV) in a water tunnel from two different facilities to examine the effects of chord Reynolds number, and the airfoil shape on the associated flow structures. Two rigid airfoils, SD7003 and flat plate, undergoing pitching and plunging motion in nominally two-dimensional conditions are investigated with the aid of the original Menter's Shear Stress Transport (SST) turbulence model and a modified version which limits the production of turbulence kinetic energy to reduce the build-up of turbulence in stagnation regions. We consider two kinematic schemes, a pitching and plunging, and a pure plunging motion. For the SD7003 airfoil under pitching and plunging motion, the original SST model offers consistently favorable agreement with both PIV measurements. For the pure plunging SD7003 airfoil case, depending on the turbulence characteristics including those caused the motion of the wing, and the implied eddy viscosity level, qualitatively different flow structures are observed experimentally and computationally. The flat plate creates flow fields insensitive to the Reynolds number, and quite different from those around the SD7003 airfoil, due to the leading edge effect.

Nomenclature

A	= pitching amplitude, in degrees
C_L	= airfoil lift coefficient per unit span
$C_{L,\mathrm{fp},10K,\mathrm{max/mean}}$	= max/mean flat plate lift coefficient per unit span at $Re = 1\times10^4$,
c	= airfoil chord (=152.4mm)
f	= airfoil oscillation pitching/plunging frequency
h	= plunging position as function of time
h_0	= non-dimensional plunging amplitude
k	= reduced frequency of pitch or plunge, $k = 2\pi fc/(2U_\infty)$

[1] Graduate Research Assistant, University of Michigan, Department of Aerospace Engineering, AIAA student member
[2] Postdoctoral Fellow, University of Michigan, Department of Aerospace Engineering, aonoh@umich.edu, AIAA member
[3] Associate Professor, University of Michigan, Department of Aerospace Engineering, lpb@umich.edu, AIAA member
[4] Aerospace Engineer, Air Vehicles Directorate, Wright-Patterson AFB, Michael.Ol@wpafb.af.mil, AIAA Associate Fellow
[5] Clarence L. "Kelly" Johnson Collegiate Professor and Chair, University of Michigan, Department of Aerospace Engineering, weishyy@umich.edu, AIAA Fellow

Re	= Reynolds number, $Re = U_\infty c/\nu$, ν taken as 10^{-6} in SI units for water at 20℃
S_{ij}	= strain-rate tensor, symmetric part of the velocity gradient tensor, i.e. $\partial u_i/\partial x_j = S_{ij} + \Omega_{ij}$
St	= Strouhal number, $St = 2fch_0/U_\infty = 2kh_0/\pi$
t/T	= dimensionless time, in fractions of one oscillation period
T	= airfoil oscillation period, $T = 1/f$
u_i	= velocity vector
U_∞	= free stream (reference) velocity
x_i	= position vector
x_p	= pitch pivot point: fraction of chord downstream from airfoil leading edge
α	= kinematic angle of incidence due to pitch
α_0	= mean angle of attack (that is, the constant pitch angle offset from zero)
α_e	= total angle of attack from trigonometric combination of pitch and plunge
ϕ	= phase difference between pitching and plunging; positive → pitch leads
λ	= ratio of pitch-amplitude to plunge-induced angle of attack
ω	= vorticity
Ω_{ij}	= vorticity tensor, anti-symmetric part of the velocity gradient tensor, see strain-rate tensor

I. Introduction

The unsteady aerodynamics of biological flapping flyers has been the subject of numerous investigations by biologists and aerodynamicists. As reviewed by Shyy *et al.*[1], important features of the aerodynamics of biological flapping flyers result from large flapping wing movement and rotation, small size, and low flight speeds. When characteristic lengths and velocities become smaller, the Reynolds number decreases. In addition, as the wing sizes decrease and flapping wing motion becomes faster, the flow field becomes more unsteady and exhibit complex flow structures. Consequently, the flow fields around the flapping wings feature the formation of large scale vortex structures, onset of separation and reattachment, near-wall pressure and velocity variations, lag between the instantaneous wing orientation, three dimensional effects, and development of the corresponding flow field[2,3,4,5,6,7]. Most of natural flapping flyers have a wide range of aspect ratio wings and flap at a Strouhal number in the range from 0.2 to 0.4[8], which suggests that fundamental features of vorticity dynamics and time-dependent aerodynamic loads must be accurately predicted. As reviewed by Shyy *et al.*[1] and reported by Tang *et al.*[9], Trizila *et al.*[11], and Wang, Birch, and Dickinson[9] for two-dimensional cases, and Shyy and Liu[12], Shyy *et al.*[4], Ramamurti and Sandberg[13], and Aono, Liang, and Liu[14] for three-dimensional cases, the fluid physics associated with the flapping wing is qualitatively and quantitatively influenced by the kinematics as well as the Reynolds number. These studies focused on the flow regime of the Reynolds number around 10^2 and 10^3, where issues such as turbulence are less dominant. In this work, we have a specific focus on the fluid physics at a higher Reynolds number regime, between 1×10^4 and 6×10^4.

Overall, the combination of low Reynolds number ($Re < 10^5$) phenomena and large topological changes in flow structure encountered in flapping wing flows suggest departure from classical unsteady airfoil theory[15]. Critical issues include the role of leading edge and trailing edge vortex shedding[16], interaction of the time dependent wing pressure distribution with shed vortices, and the role of transition in shear layers bounding regions of laminar separation[17,18]. Prior to current interest in flapping wing aerodynamics, dynamic stall of helicopter blades was perhaps the main application for high-rate unsteady aerodynamics in a nominally two dimensional wing, but the Reynolds number is much higher. It was established that the dominant feature of dynamic stall is the formation and shedding of a strong vortex-like disturbance near the leading edge. McCroskey *et al.*[19] pointed out that as the vortex passes over the airfoil surface, it significantly changes the chordwise pressure distribution and produces transient forces and moments that are fundamentally different from those in static stall. Comprehensive reviews of dynamic stall are given by McCroskey[20], Carr[21], and Carr and McCroskey[22]. Ohmi *et al.*[23,24] experimentally examined the starting flows past a two-dimensional oscillating and translating airfoil, finding that the reduced frequency is the dominant parameter of the flow. However, they also demonstrated that as the pitching frequency increases, the patterns of the vortex wake are dependent on both the reduced frequency and the amplitude. Visbal and Shang[25] performed numerical investigations of the flow structure around a rapidly pitching NACA0015 airfoil at Reynolds number of 10^4 by solving the full two-dimensional Navier-Stokes equations. They observed a strong dependence of the

primary flow features on the pitch rate and pitch pivot point location. At a fixed axial location, the dynamic stall can be delayed with increased pitch rate, suggesting that lags between evolution of flow separation and the airfoil motion kinematics should increase with increasing reduced frequency. Choudhuri and Knight[26] examined the effects of compressibility, pitch rate, and Reynolds number on the initial stages of two-dimensional unsteady separation of laminar subsonic flow over a pitching airfoil in the Reynolds numbers ranging from 10^4 to 10^5, finding that increasing the Reynolds number hastens the appearance of the primary recirculating region.

The afore-mentioned studies focus mostly on transients following the initiation of the airfoil motion from the rest. Others considered the periodic or phase-averaged behavior of pitch/plunge motions after initial transients have relaxed, typically with a focus on motion kinematics for optimal thrust efficiency. Platzer and Jones[27] discussed theoretical prediction of thrust efficiency compared with flow visualization and thrust measurements for an airfoil in pure plunging motion over a wide range of reduced frequencies and reduced amplitudes. Young and Lai[28] used a two-dimensional Reynolds-Averaged Navier-Stokes (RANS) approach to study the frequency-amplitude parameter space for optimal thrust efficiency. Lian and Shyy[29] used RANS methods to study the effect of an abstraction of gusts on a pitching/plunging airfoil, with evidence that the flapping motion has gust load alleviation potential, and that gusts can cause hysteresis in the force history and affect the transition process. Visbal, Gordnier, and Galbraith[30] performed high-fidelity implicit large-eddy simulations to investigate three-dimensional unsteady fluid physics around a SD7003 airfoil plunging at reduced frequency of 3.93.

Lentink and Gerritsma[31] considered different airfoil shapes numerically to investigate the role of shapes on the aerodynamic performance. They computed flow around hovering airfoils at $Re = O(10^2)$, and concluded that the thin airfoil with aft camber outperformed other airfoils including the more conventional airfoil shapes with thick and blunt leading edges.

In this paper we conduct an extended investigation of previous studies by Kang, *et al.*[32], and Ol, *et al.*[33]. We study the numerical modeling aspects on the flow field of nominally two-dimensional airfoils undergoing combined pitching and plunging at Reynolds numbers 1×10^4, 3×10^4, and 6×10^4. The two different sets of kinematics represent a weak dynamic stall (under combined pitching-plunging) and a stronger dynamic stall (under pure plunging), respectively. Two different foils are considered: the SD7003 airfoil and a flat plate with 2.3% thickness. Experimental and computational flow field results are compared: two versions of Menter's Shear Stress Transport (SST) turbulence closures for two-dimensional RANS computations, and phase-averaged Particle Image Velocimetry (PIV) measurements. The focus of the investigation is (i) to understand the fluid physics observed in the experiments, (ii) to qualitatively and quantitatively ascertain the performance of RANS computations, aimed at aiding engineering design, and (iii) to probe the implications of the Reynolds number, kinematics, and airfoil shapes. The experiments were recently obtained in two different facilities, one at the Air Vehicle Directory of the Air Force Research Laboratory (AFRL) and the other at Department of Aerospace Engineering of the University of Michigan (UM). The consistency and inconsistency of the experimental as well as computational endeavors offer significant opportunities for us to probe the modeling and experimental implications, and the interplay between fluid physics and geometry and pitch-plunge motion under different Reynolds number.

II. Experimental, and Computational Setup

A. Experimental Approach

Experimental data are obtained through 2-component digital particle image velocimetry (DPIV) experimental technique from both facilities: AFRL Horizontal Free-surface Water Tunnel (HFWT) and University of Michigan Low-Turbulence Water Channel, see Ol *et al.*[33], and Baik *et al.*[34], for the detailed discussion on the experimental setup, respectively. The SD7003 airfoil model, and flat plate model with rounded leading and trailing edge are mounted less than 1 mm from the wall in order to minimize the three-dimensional effect. The model used in HFWT has approximately 15 cm shorter span due to shorter test section width. The main difference between the two facilities is in the model mounting scheme which brought different levels of tunnel free-surface and blockage effects. A short comparison between the two facilities is tabulated in Table 1.

Table 1. Similarity and differences between the two facilities (UM Water Channel and AFRL HFWT).

	UM Water Channel	AFRL HFWT
Test section height (cm)	61	61
Test section width (cm)	61	46
SD7003 airfoil chord (cm)	15.2	15.24
SD7003 airfoil span (cm)	60.0	45.7
Flat plate chord (cm)	15.2	15.24
Flat plate span (cm)	60.1	45.7
Wall-to-airfoil gap (cm)	< 0.1	< 0.1
Particle seeding	3 micron diameter TiO_2	2~3 micron diameter TiO_2
Freestream turbulence intensity	< 1%	0.4 – 0.5%
Model mounting scheme	Wall-to-endplate vertical cantilevered mount with endplate just below the water surface	Wall-to-wall horizontal mount with vertical support rods at the center of test section

B. Computational Approach

The governing equations for the numerical simulation are the RANS equations coupled with Menter's SST model[37, 38], and the continuity equation for incompressible flow,

$$\frac{\partial}{\partial x_i}(u_i) = 0$$

$$\frac{\partial}{\partial t}(u_i) + \frac{\partial}{\partial x_j}(u_j u_i) = -\frac{1}{\rho}\frac{\partial p}{\partial x_i} + \frac{\partial}{\partial x_j}\left\{(\nu + \nu_t)\frac{\partial u_i}{\partial x_j}\right\}$$

$$\nu_t = \frac{a_1 k}{\max(a_1\omega, S F_2)}$$

$$\tau_{ij} = \rho\nu_t\left(\frac{\partial u_i}{\partial x_j} + \frac{\partial u_j}{\partial x_i}\right) - \frac{2}{3}\rho k\delta_{ij}$$

$$\frac{\partial k}{\partial t} + \frac{\partial}{\partial x_j}(u_j k) = \hat{P}_k - \beta^*\omega k + \frac{\partial}{\partial x_j}\left\{(\nu + \sigma_k\nu_t)\frac{\partial k}{\partial x_j}\right\} \quad (1)$$

$$\frac{\partial \omega}{\partial t} + \frac{\partial}{\partial x_j}(u_j \omega) = -\frac{\gamma}{\nu_t}\frac{\tau_{ij}}{\rho}\frac{\partial u_i}{\partial x_j} - \beta\omega^2 + \frac{\partial}{\partial x_j}\left\{(\nu + \sigma_\omega\nu_t)\frac{\partial \omega}{\partial x_j}\right\}$$

where a_1, β, β^*, γ, σ_k, σ_ω,F_2 are defined as in Menter's SST formulation[37], u_i is the velocity component in the i^{th} direction, x_i is the i^{th} component of the position vector, t is time, ρ is density, p is pressure, ν is the kinematic viscosity, ν_t is the eddy viscosity, $S = \sqrt{2S_{ij}S_{ij}}$ is the invariant measure of the strain rate. Compared to Menter's original SST turbulence model a limiter has been built in to the production term, $\hat{P}_k$, in the turbulence kinetic energy (TKE) equation, Eq. (1), as

$$P_k = \mu_t\frac{\partial u_i}{\partial x_j}\left(\frac{\partial u_i}{\partial x_j} + \frac{\partial u_j}{\partial x_i}\right),$$
$$\hat{P}_k = \min(P_k, 10\cdot\beta^*\rho k\omega),$$

where P_k is the production term in the original SST formulation, to prevent the build-up of turbulence in stagnation regions. Another change is the use of invariant measure of the strain-rate tensor in the formulation

for the eddy viscosity instead of the vorticity magnitude, $\Omega = \sqrt{2\Omega_{ij}\,\Omega_{ij}}$. The strain-rate invariant is considered to be a better measure for the fluid deformation, since the Boussinesq approximation is also based on the strain-rate. The two differences between the original and the modified SST formulation are summarized in Table 2.

These equations are solved with the in-house solver Loci-STREAM[39]. Loci-STREAM is a parallelized unstructured curvilinear pressure-based finite-volume code with moving grid capabilities. The present calculations uses implicit first order time stepping. The convection terms are treated using the second order upwind scheme[40, 41] while pressure and viscous terms are treated using second order schemes. The geometric conservation law[42, 43], a necessary consideration in domains with moving boundaries, is satisfied.

Table 2 Original[38] and modified[37] SST turbulence model

	Original SST	Modified SST
Production term of TKE equation	$P_k = \mu_t \frac{\partial u_i}{\partial x_j}\left(\frac{\partial u_i}{\partial x_j} + \frac{\partial u_j}{\partial x_i}\right)$	$\hat{P}_k = \min(P_k, 10 \cdot \beta^* \rho k \omega)$
Eddy viscosity	$\nu_t = \frac{a_1 k}{\max(a_1 \omega, \Omega F_2)}$	$\nu_t = \frac{a_1 k}{\max(a_1 \omega, \mathrm{S} F_2)}$

The numerical solutions are computed in open bounded domain with Loci-STREAM on an unstructured grid with 46281, and 32204 mixed elements for the SD7003 airfoil, and flat plate, respectively, see Figure 1. The outer boundaries of the computational domain are 50 (Figure 1(a1)), and 30 chord lengths apart (Figure 1(b1)), respectively. The thickness of the flat plate is 2.3% chord length and the leading and trailing edges are rounded (radius of 1.15 % chord length). The boundary conditions are as follows: on the airfoil no-slip conditions are imposed; the outer boundaries are incompressible inlets; and the inlet turbulence intensity is 0.5%. The computations are run assuming fully-turbulent, with no attempt to model transition or to prescribe the chordwise location of when to turn on the production term in the turbulence model.

The spatial and temporal sensitivity studies are shown in Appendix A.

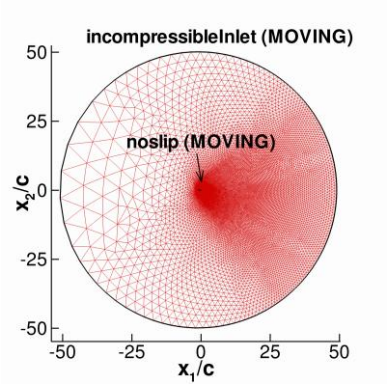

(a1) SD7003 airfoil in open bounded domain

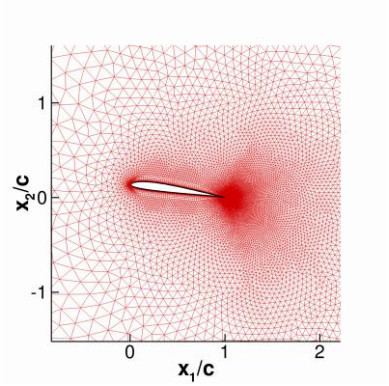

(a2) Mixed elements near the SD7003 airfoil

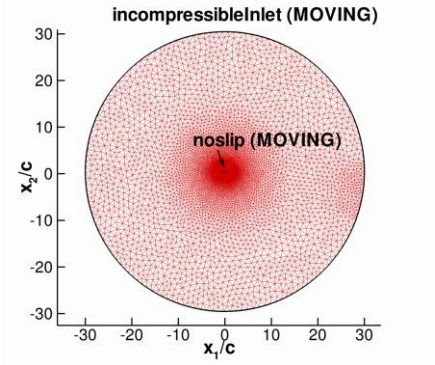

(b1) Flat plate airfoil in open bounded domain

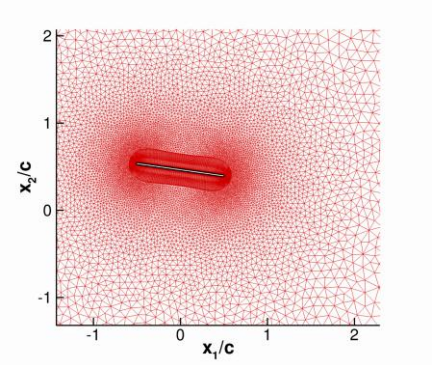

(b2) Mixed elements near the flat plate

Figure 1. Computational grid systems: (a) SD7003; (b) Flat plate.

C. Case Description

The motion kinematics time histories are described by

$$h(t) = h_0 c \cos(2\pi t/T)$$
$$\alpha(t) = \alpha_0 + A\cos\{2\pi(t/T + \phi)\}$$

where h is the location of the center of rotation (x_p/c = 0.25) of the airfoil measured normal to the free stream, h_0 is the normalized amplitude of the plunge motion, T is the motion physical period, c is the airfoil chord, α is the geometrical angle of attack (AoA) measured relative to the incoming free stream with velocity, U_∞, α_0 is the mean angle of attack, and A is the amplitude of the pitching motion, see Figure 2.

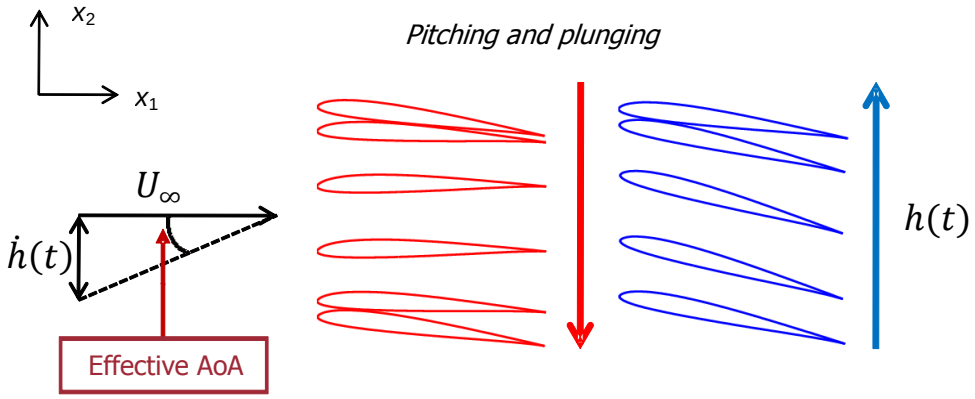

Figure 2. Schematic of SD7003 airfoil positions in downstroke (RED) and upstroke (BLUE), and the definition of the free stream direction and the effective angle of attack (effective AoA) due to plunging motion.

The effective angle of attack, α_e, is a linear combination of the pitching angle and the induced angle due to plunging motion, and can be written as,

$$\alpha_e = \alpha_0 + \lambda \arctan(\pi St)\cos\{2\pi(ft + \phi)\} + \arctan\{\pi St \sin(2\pi ft)\}$$

where $St = 2fch_0/U_\infty$ is the Strouhal number, and $\lambda = A/\arctan\{\max(\dot{h})/U_\infty\}$ is the ratio of the maximum effective angles of attack of the pitching motion to the plunge motion, where $\dot{h}$ is the plunge velocity, see Figure 3. The Reynolds number is varied by changing the flow speed, $Re = U_\infty c/\nu$. It is clear from the kinematics that maintaining the same effective angle of attack time history requires a constant Strouhal number and constant λ. Thus, as Re varies, the reduced frequency, $k = \pi fc/U_\infty = \pi St/(2h_0)$, and the Strouhal number are kept constant by varying the physical frequency proportionately.

The choice of reduced frequency, k = 0.25, is motivated in part by cruise-type conditions for flapping flight of bird. Although the corresponding Strouhal number, St = 0.08, is below the range for maximum propulsion efficiency[46], the present flow conditions are on the upper-end of the dynamic-stall literature, where the main application is helicopter blade aerodynamics[20,47], and for which the traditional analytical or phenomenological models in aeronautics tend to focus. As is often taken in applications motivated by maximizing propulsive efficiency of pitching and plunging motion[46], pitching leads plunging by one quarter of motion period: phase ϕ = 0.25 and thus the airfoil "feathers", with the geometric pitching angle partially cancelling the plunge-induced angle of attack, $\arctan(\dot{h}/U_\infty)$. The pitching amplitude, A, is computed from the value of λ= 0.6 for the combined pitching and plunging case, while for the pure plunging case, λ =0. The total effective angle of attack time-trace, α_e, straddles the static stall value of approximately 11° [48]; this is just the sum of the pitching and plunging angles with appropriate phase shift.

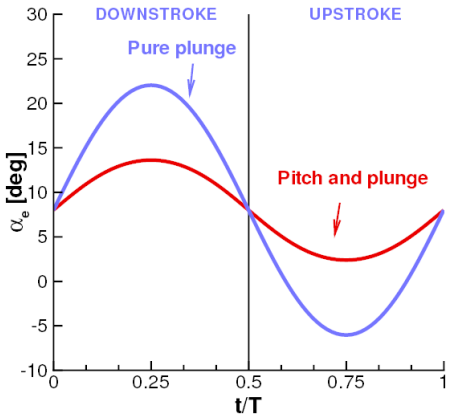

Figure 3. Time history of effective angle of attack (α_e) for the pitching and plunging kinematics (red line) and the pure plunging kinematics (blue line).

III. Results and Discussion

A. Flow around a SD7003 Airfoil at $Re = 6\times10^4$

1. Pitching and Plunging Case

In the previous study[32] the numerical solution using the original SST turbulence closure showed an excellent agreement with the experimental data (UM) at this Reynolds number qualitatively, and quantitatively.

Figure 4 shows the normalized mean streamwise velocity, u_1/U_∞, contours along with planar streamlines from the numerical and the experimental results from the UM and AFRL at t/T = 0.00, 0.25, 0.42, 0.50, and 0.75, respectively. The numerical solution with the modified SST turbulence model overpredicts the separation leading to generation of vortical structures at the bottom of the downstroke, t/T = 0.50, which is not observed in both PIV data. This is also illustrated in Figure 5, which shows u_1/U_∞-component velocity profiles at four different time instants at constant x_1/c = 0.25.

The overprediction of separation when using the modified SST model could be explained by the use of a limiter for the production term in the TKE equation. The build-up of turbulence near stagnation flow region is prevented, reducing the eddy viscosity in the RANS model. Figure 6 shows the local Reynolds number contours defined as $U_\infty c/(\nu + \nu_t)$ from the numerical computations using both SST turbulence closures at t/T = 0.25 for the pitching and plunging SD7003 airfoil. The limiter of the production in the TKE equation, see Eq. (1), enforced in the modified SST model results in substantially lower eddy viscosity, and hence higher local Reynolds number. Using the original SST turbulence model the viscosity ratio is at maximum near the leading edge. For the modified SST model, by limiting the production of TKE the local Reynolds number near the leading edge of the airfoil is close to 6×10^4, i.e. the amount of eddy viscosity in this region of the flow is small. Hence the flow tends to separate near the leading edge which is observed at t/T = 0.42 and 0.50 in Figure 4.

On the other hand, the agreement between the two experimental measurements is excellent, both in streamwise velocity contours as well as in streamlines. During the downstroke motion the numerical solution with the modified SST model tends to predict larger reversed flow regions. The flow exhibits separation between the center of the downstroke and the bottom of the downstroke (Figure 4), corresponding to the maximum instantaneous effective angle of attack of 13.6°. Note that this value for the effective angle of attack is well beyond the static stall angle of 11°.

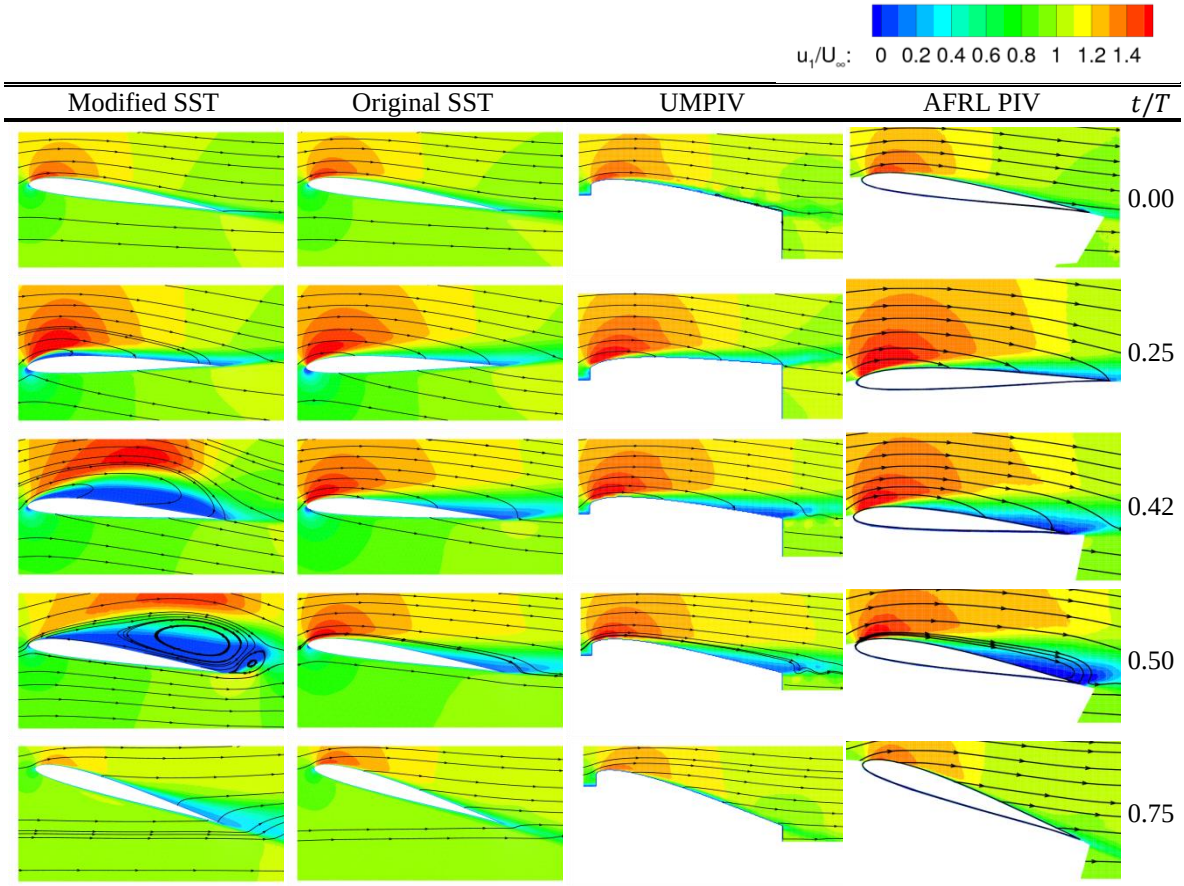

Figure 4. u_1/U_∞ contours and the instantaneous streamlines over pitching and plunging SD7003 airfoil at k = 0.25, λ =0.6, and at Re = 6×10^4 from numerical (Modified SST, Original SST), and experimental (UM, AFRL) results.

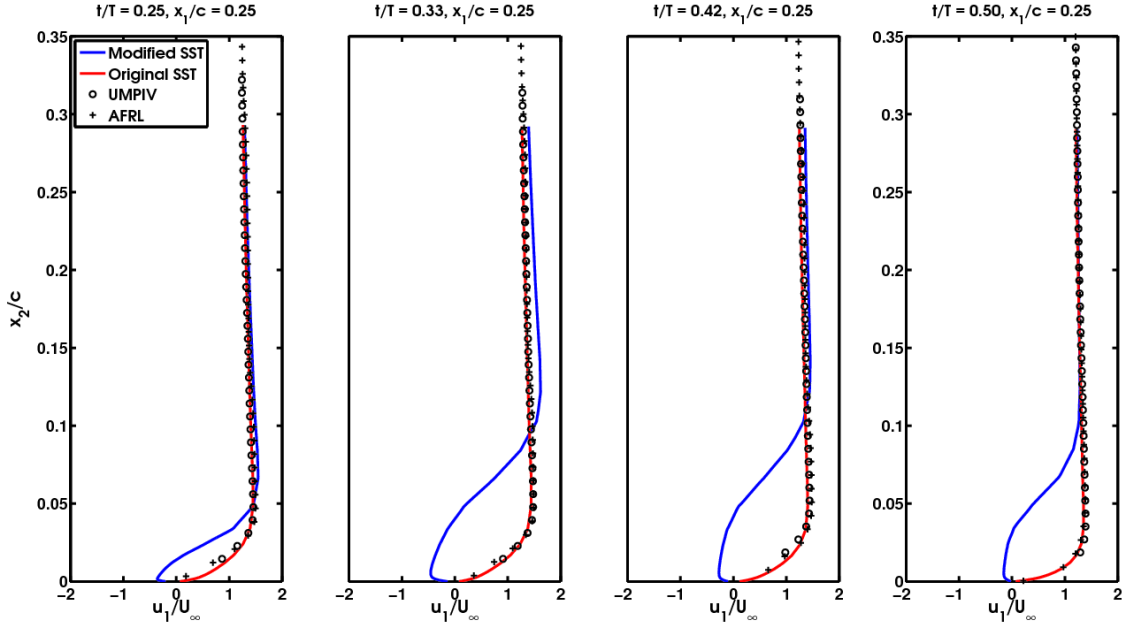

Figure 5. u_1/U_∞ profiles from numerical (Modified SST, Original SST), and experimental (UM, AFRL) results at t/T = 0.25, 0.33, 0.42, and 0.50 at constant x_1/c = 0.25 at Re = 6×10^4, k = 0.25, λ =0.6 for the pitching and plunging SD7003 airfoil.

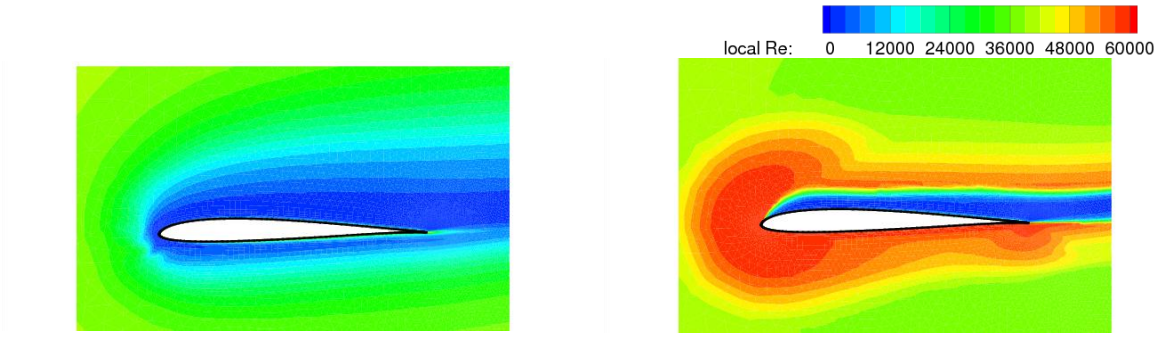

(a) Original SST (b) Modified SST

Figure 6 Local Reynolds number contours using (a) the original SST, and (b) the modified SST at t/T = 0.25 for pitching and plunging SD7003 airfoil at Re = 6×10^4, k = 0.25, λ =0.6.

2. Pure plunging case

Using the original version of SST turbulence model the computation showed a thinner but open separation[32], however the approach with the modified version of SST model the numerical result is able to predict the vortical structure with reattachment at x_1/c ~ 0.8 at t/T = 0.25.

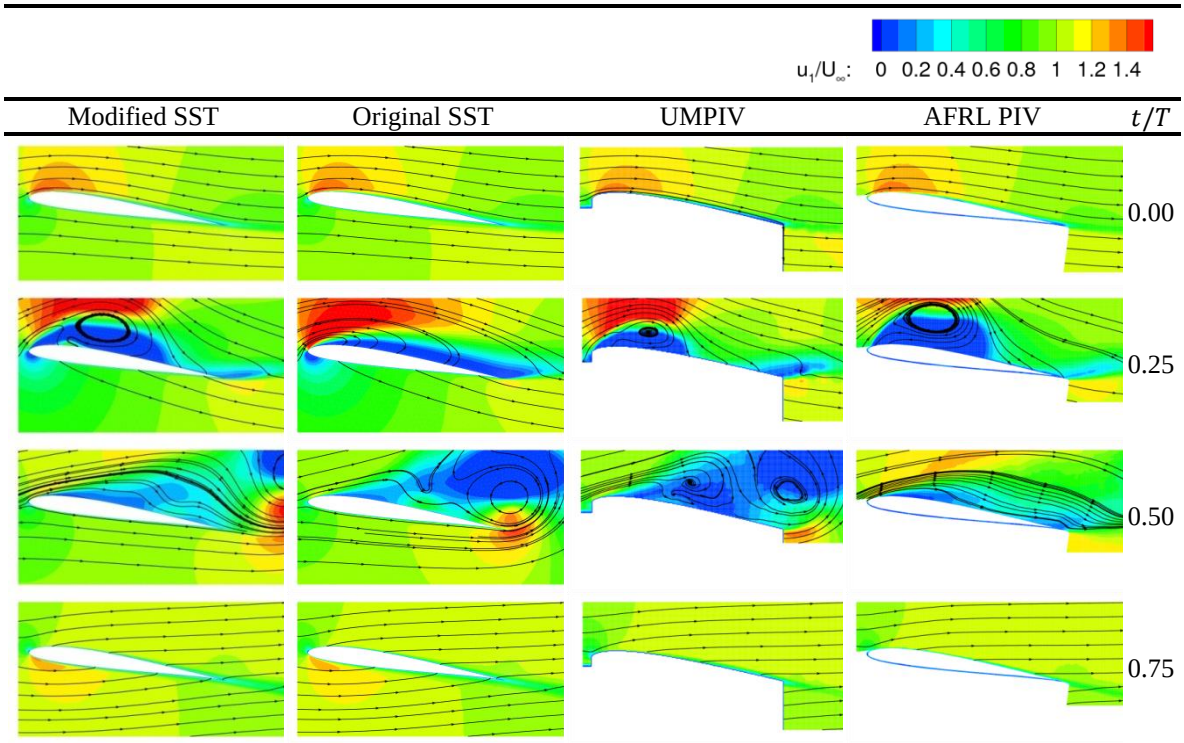

Figure 7. u_1/U_∞ contours and instantaneous streamlines over pure plunging SD7003 airfoil at k = 0.25, λ =0.0, and at Re = 6×10^4 from numerical (Modified SST, Original SST), and experimental (UM, AFRL) results.

Figure 7 shows the u_1/U_∞ contour plots and the instantaneous streamlines from the numerical computation and the experimental measurements from the UM and AFRL water tunnels for the pure plunging SD7003 airfoil at t/T = 0.00, 0.25, 0.50, and 0.75. The agreement between the computational and the experimental approaches is favorable when the flow is largely attached. When the flow exhibits massive separation, for example at t/T = 0.50, the experimental and computational results show noticeable differences in phase as well as the size of flow separation. The details of the vortical structures differ in all results; however, it is interesting to observe that the original SST model matched the PIV results from the UM facility better, while the modified SST model produced result more consistent with that from the AFRL

facility. The consistent/inconsistent results appeared at t/T = 0.50 where a smaller vortical structure is evinced on the suction side of the airfoil in the UM facility, while in AFRL data such a vortical structure is hardly present.

As already discussed, the flow tends to separate more substantially under the modified SST model than under the original SST model due to different eddy viscosity levels predicted. The exact cause of the difference between the two PIV data is not clear right now. Based on the computational assessment, the effective inlet turbulence level of the two tunnels associated with the wing motion may be different. The differences in the experimental setup, i.e. mounting schemes, and tunnel dimensions, are tabulated in Table 1.

B. Reynolds Number Effect on Pitching and Plunging SD7003 Airfoil: $Re = 1\times10^4$, 3×10^4, and 6×10^4

The pitching and plunging case is conducted at three different Re: 1×10^4, 3×10^4 and 6×10^4 to assess the effect of Reynolds number on the fluid physics.

At $Re = 3\times10^4$, the comparison between the experiment (UM) and the numerical simulations are similar to that at $Re = 6\times10^4$: the numerical simulation with the modified SST closure predicts flow separation similar to the structures shown in Figure 6, while the experimental data, and numerical computation using the original version of SST show mostly attached flow, see Figure 10. The reason behind this discrepancy can be explained by the same reasoning used for $Re = 6\times10^4$ case; the modified SST model limits the production of turbulence kinetic energy hence reducing the eddy viscosity.

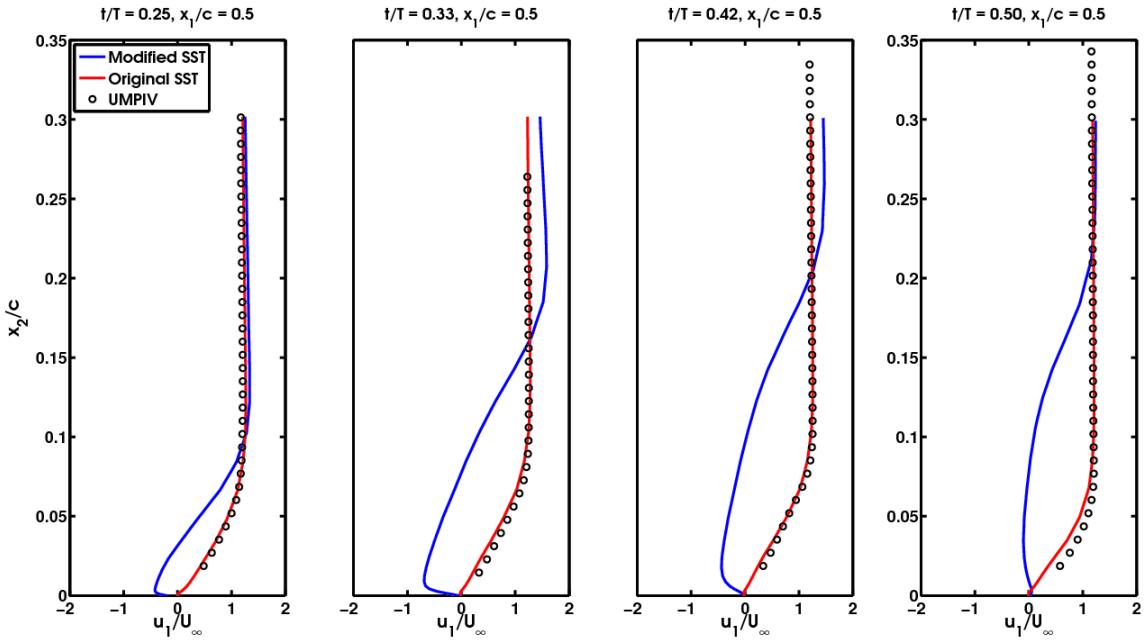

Figure 8 u_1/U_∞ profiles from the numerical (Modified SST, Original SST), and experimental (UM) results at t/T = 025, 0.33, 0.42, and 0.50 at constant x/c = 0.50 at $Re = 3\times10^4$, k = 0.25, λ =0.6 for the pitching and plunging SD7003 airfoil.

At $Re = 1\times10^4$, numerical simulation predicts a layer of reversed flow throughout the length of the chord. The experimental data acquired at UM facility show reversed flow at the wall and a boundary layer of similar thickness. Both numerical prediction of the flow separation near the leading edge agrees well with the experimental data. In the contour plots of the experimental data, multiple vortical structures are observed during middle of downstroke, see Figure 9(c, e), which are not present in other Reynolds numbers considered. Figure 9(a) plots u_1/U_∞-component velocity profiles at four time instants at a constant downstream location as indicated. At t/T = 0.25 and 0.33 the u_1/U_∞-component velocity profile of the experimental data overshoots when recovering back to the freestream velocity magnitude. This overshoot could be explained by noticing the presence of the small vortical structures shown in the u_1/U_∞ contour plots. Furthermore, at $Re = 1\times10^4$, the flow from both SST models evinces similar u_1/U_∞ velocity profiles with reversed flow regions

near the airfoil. At this Reynolds number the sum of eddy viscosity and laminar viscosity is comparable in the results using both turbulence closures due to weaker turbulence strength.

Figure 10 shows the time histories of lift coefficient for the Reynolds numbers considered using the original SST turbulence model. The influence of the Reynolds number on the global trend and the maximum lift coefficient is slight, however at Re = 1×10^4 the lift drop between t/T = 0.42 and 0.75 is noticeably different than at other Reynolds numbers. This is because at Re = 1×10^4 flow separates on the suction side of the airfoil while at Re = 6×10^4 and 3×10^4 the flow is mostly attached.

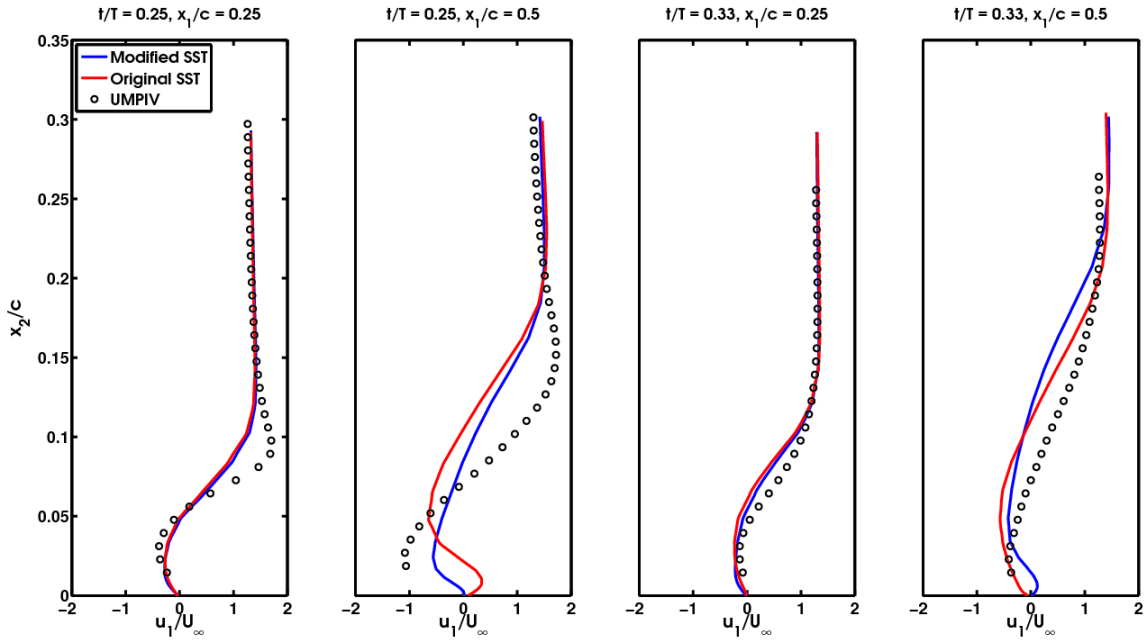

(a) u_1/U_∞ profiles from numerical (Modified SST, Original SST), and experimental (UM) results at constant $x_1/c = 0.25$ at t/T = 0.25, 0.33, 0.42, and 0.50.

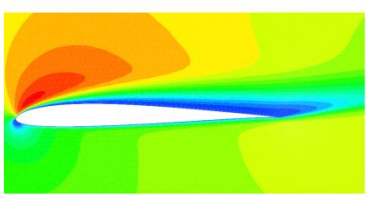

(b) u_1/U_∞ contour at t/T = 0.25, original SST

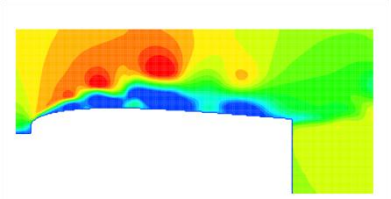

(c) u_1/U_∞ contour at t/T = 0.25, UMPIV

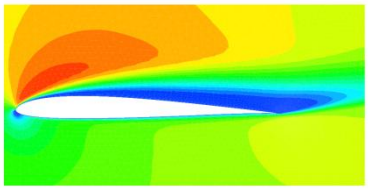

(d) u_1/U_∞ contour at t/T = 0.33, original SST

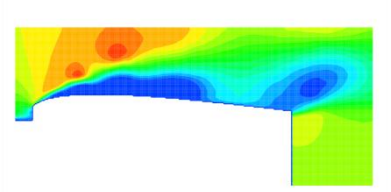

(e) u_1/U_∞ contour at t/T = 0.33, UMPIV

Figure 9. u_1/U_∞ profiles and contours from numerical (Modified SST, Original SST), and experimental (UM) results at Re = 1×10^4, k = 0.25, λ =0.6for the pitching and plunging SD7003 airfoil.

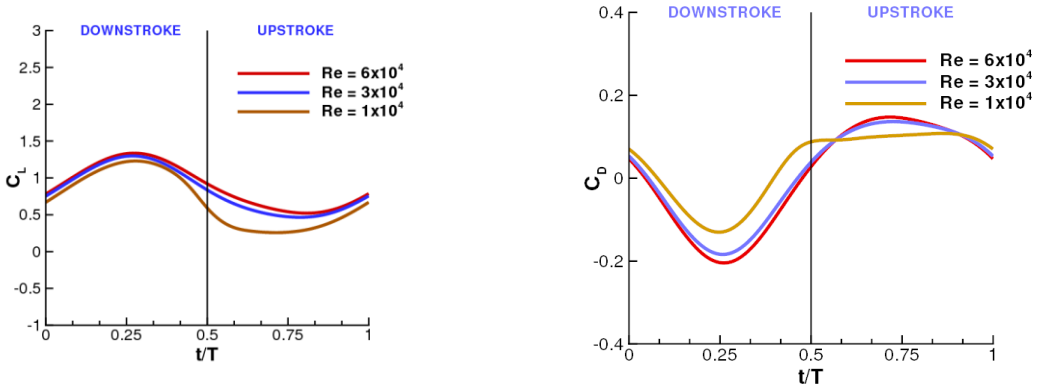

(a) lift coefficient (b) drag coefficient

Figure 10. Time histories of (a) lift coefficient and (b) drag coefficient for the pitching and plunging SD7003 airfoil for Re = 1×10^4, 3×10^4, and 6×10^4 (k = 0.25, λ=0.6). Note that numerical solution is obtained using the original SST turbulence model.

C. Flow around Flat Plate at Re = 1×10^4, 3×10^4, and 6×10^4

1. Pitching and plunging case

The pitching and plunging case for two-dimensional flat plate is conducted at three different Re: 1×10^4, 3×10^4, and 6×10^4 numerically, and experimentally (UM). The PIV data at AFRL are only taken at Re = 6×10^4. Figure 11 shows the comparison of the numerical computation with the PIV measurements at Re = 6×10^4. Qualitatively all u_1/U_∞ contours agree well. In the experiment the leading edge separation, and the vortical structure generated as the effective angle of attack increases, has phase delay compared to the numerical results as shown by the location of the maximal accelerated flow region at t/T = 0.25, and 0.50. Furthermore, the leading edge effect overwhelms the difference between turbulence models.

The differences between results in Figure 11 using the original and the modified SST turbulence model are small. Figure 12 shows the local Reynolds number contours from the computations using both SST turbulence closures at t/T = 0.25 for the pitching and plunging flat plate. Similar eddy viscosity effects as in Figure 6 are observed that the eddy viscosity level in the result using the modified SST model is lower at the leading edge compared to the computation using the original version of SST. However, in the critical regions above the plate, the two models produce comparable eddy viscosity distributions due to the leading edge effect. Consequently, the resulting flow structures from the two models are similar as well.

Figure 13 shows the u_1/U_∞ profiles along x_2/c at constant x_1/c locations on the flat plate at t/T = 0.00 where the both numerical results show the largest reversed flow region, followed by the PIV measurements in AFRL. The flow reattaches before x_1/c = 0.25 in the UM experimental data. The results from all approaches agree well in the wake region.

At t/T = 0.00 when the flow is attached the viscosity plays a role in shaping the normalized streamwise velocity profile as shown in Figure 14. In Figure 14 three Reynolds numbers, Re = 1×10^4, 3×10^4, and 6×10^4 have been considered numerically (modified SST) and experimentally in the UM facility. At x_1/c = 0.25 the u_1/U_∞ profiles from the experiments at Re = 6×10^4 shows attached flow, and at Re = 1×10^4 separated flow. On the other hand, when the flow is largely separated as at t/T = 0.50, see Figure 15, the influence from the Reynolds number is negligible, and the numerical computation using the original SST turbulence closure agrees well with the PIV measurements in UM.

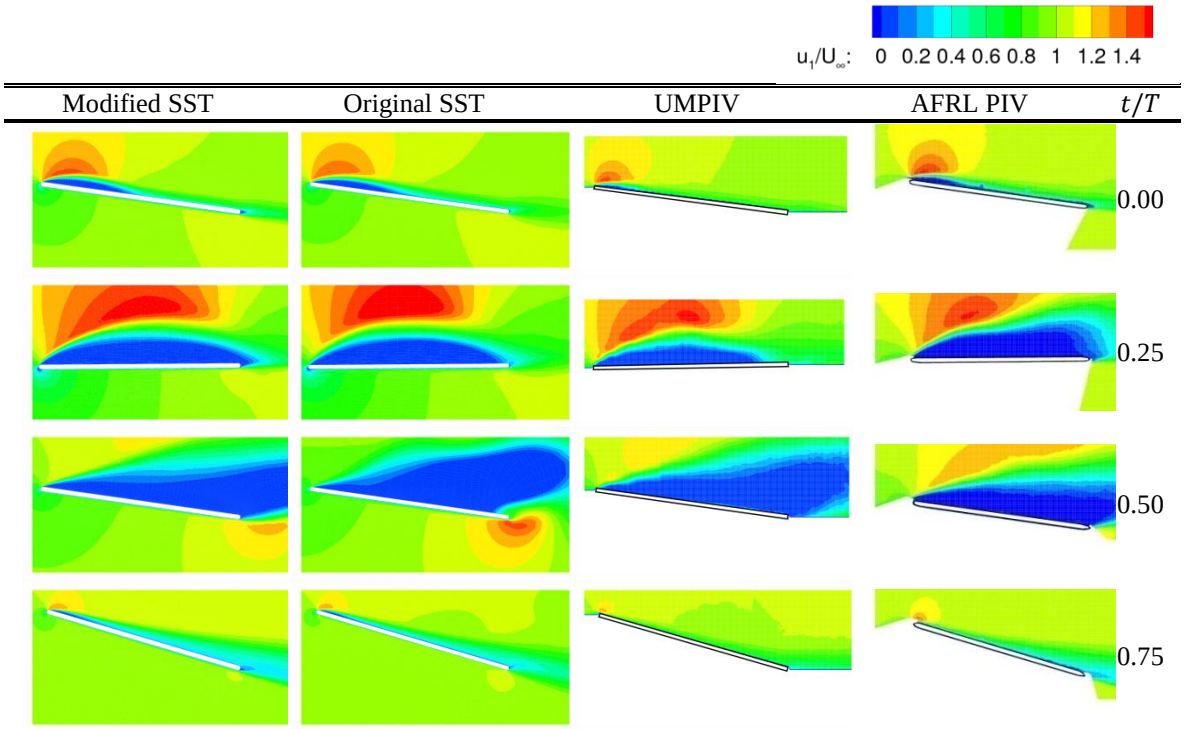

Figure 11 u_1/U_∞ contours around the pitching and plunging flat plate at k = 0.25, λ = 0.6, and Re = 6×10^4 from numerical (Modified SST, Original SST), and experimental (UM, AFRL) results at t/T = 0.00, 0.25, 0.50, and 0.75.

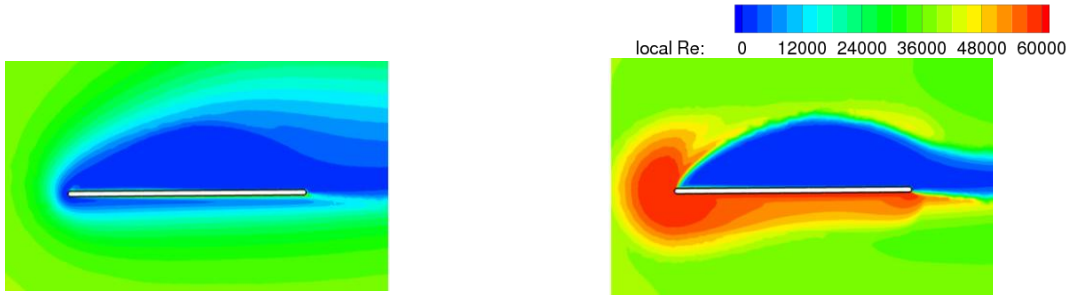

(a) Original SST (b) Modified SST

Figure 12 Local Reynolds number contours using (a) the original SST, and (b) the modified SST at t/T = 0.25 for pitching and plunging flat plate at Re = 6×10^4, k = 0.25, λ =0.6.

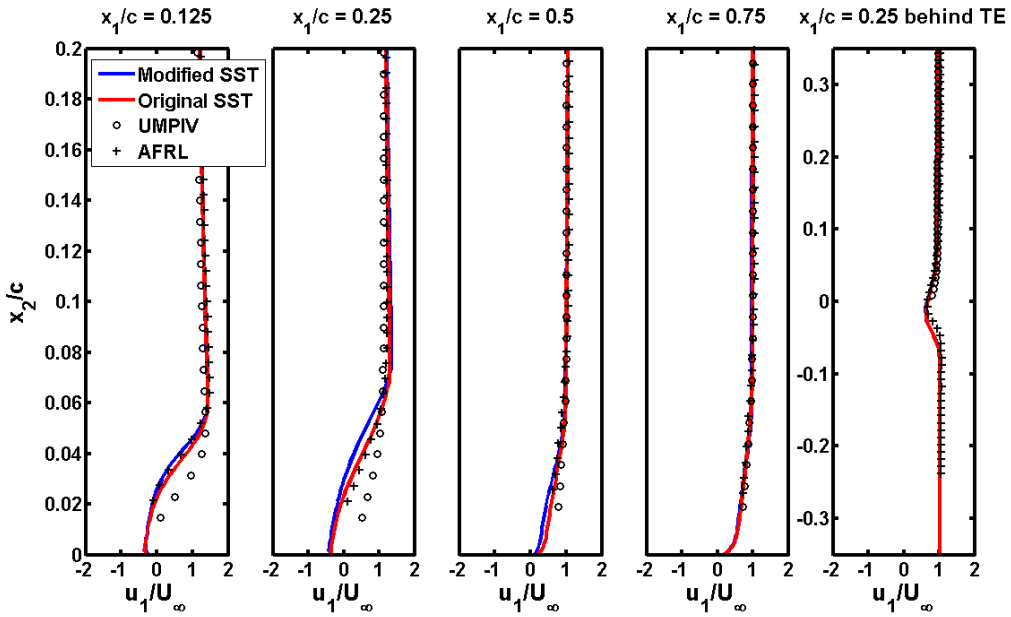

Figure 13 u_1/U_∞ profiles from the numerical (Modified SST, Original SST), and experimental (UM, AFRL) results at constant x_1/c = 0.125, 0.25, 0.50, 0.75, and 0.25 behind the trailing edge at t/T = 0.00 at Re = 6×10^4, k = 0.25, λ =0.6 for the pitching and plunging flat plate.

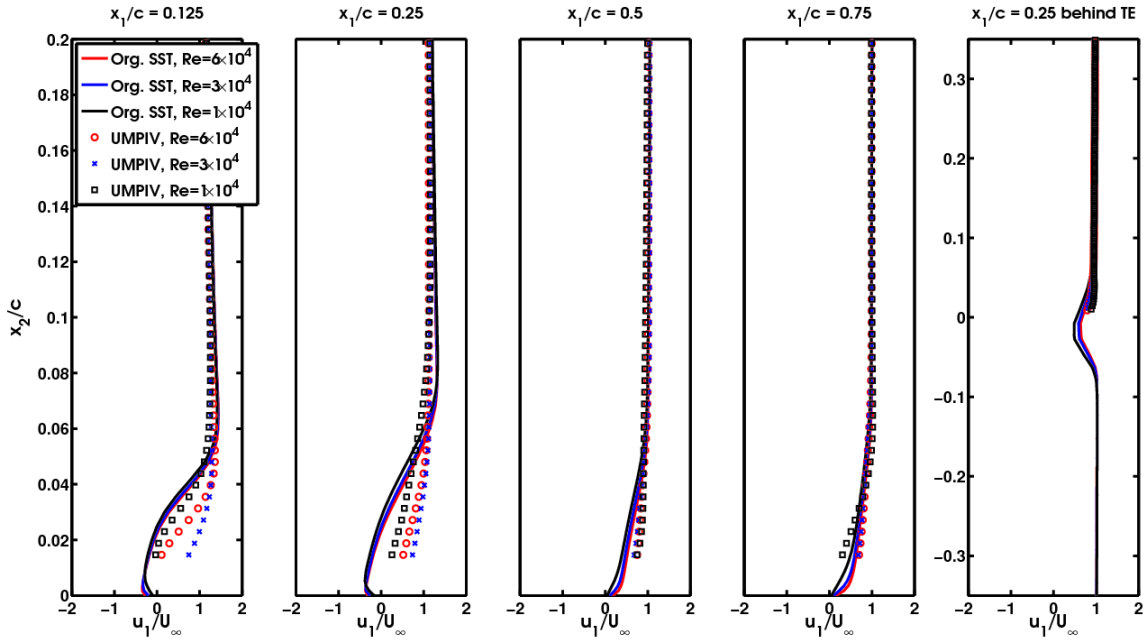

Figure 14 u_1/U_∞ profiles from the numerical (original SST) and experimental (UM) results at constant x_1/c = 0.125, 0.25, 0.50, 0.75, and 0.25 behind the trailing edge at t/T = 0.00 at Re = 1×10^4, 3×10^4, and 6×10^4, k = 0.25, λ =0.6 for the pitching and plunging flat plate.

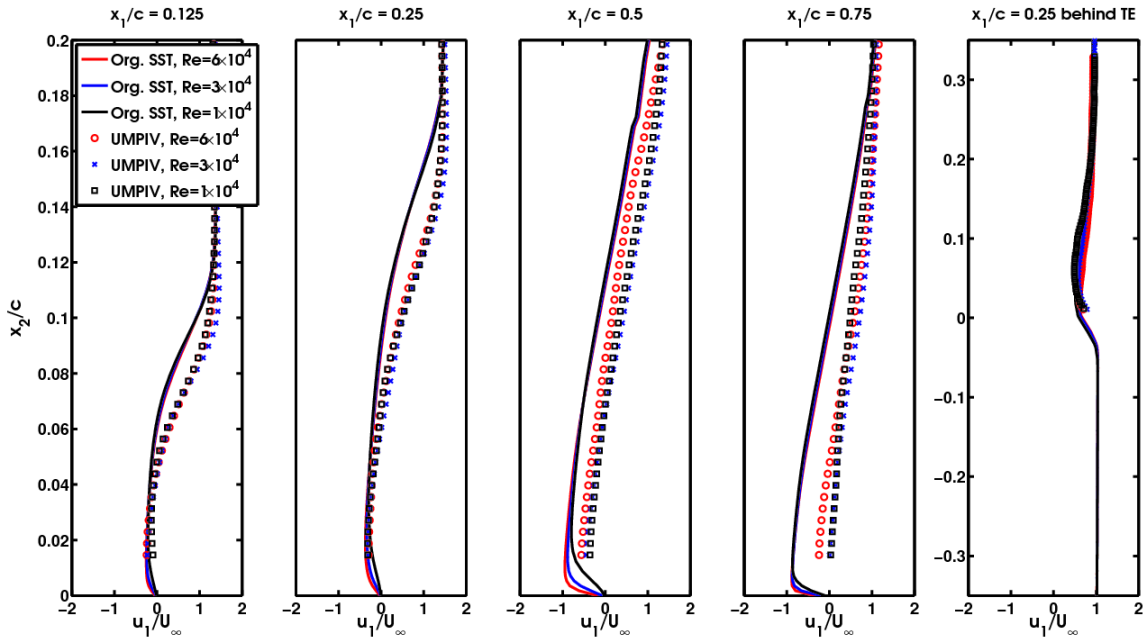

Figure 15 u_1/U_∞ profiles from the numerical (original SST) and experimental (UM) results at constant x_1/c = 0.125, 0.25, 0.50, 0.75, and 0.25 behind the trailing edge at t/T = 0.50 at Re = 1×10^4, 3×10^4, and 6×10^4, k = 0.25, λ =0.6 for the pitching and plunging flat plate.

The time histories of lift coefficient, and drag coefficient from the numerical computations (original SST) are shown in Figure 16. Both coefficients are on top of each other for Re = 3×10^4, and 6×10^4 indicating that the Reynolds number effect is minimal for these kinematics. At Re = 1×10^4 the maximum of lift coefficient around t/T = 0.25 occurs slightly earlier and is smaller in magnitude: $C_{L,\,\mathrm{fp,10K,\,max}}$= 2.50, than for Re = 6×10^4 ($C_{L,\,\mathrm{fp,60K,\,max}}$= 2.55), and 3×10^4 ($C_{L,\,\mathrm{fp,60K,\,max}}$=2.55). Similarly the time histories of drag coefficient for Re = 3×10^4, and 6×10^4 coincide whereas for Re = 1×10^4 the drag is slightly larger between t/T = 0.25 to 1.0.

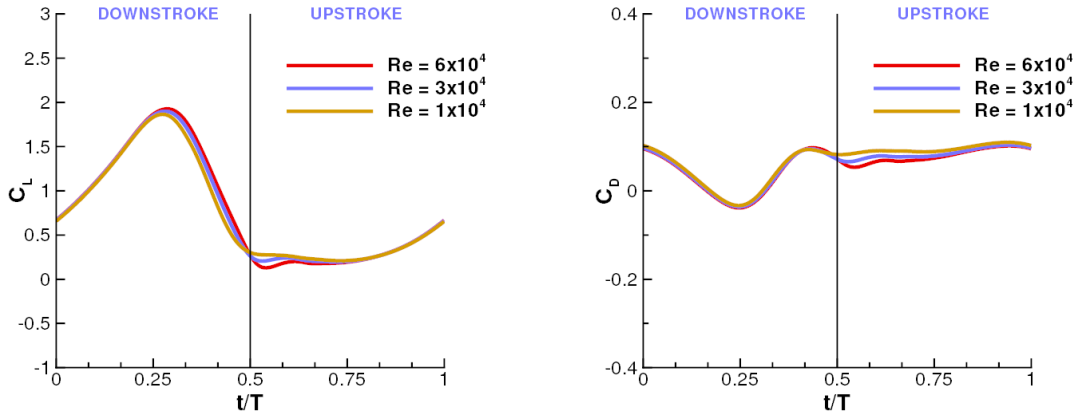

(a) lift coefficient (b) drag coefficient

Figure 16. Time histories of (a) lift coefficient and (b) drag coefficient for a flat plate at k = 0.25, and λ = 0.6 for Re = 1×10^4, 3×10^4, and 6×10^4. Note that numerical solution is obtained using the original SST turbulence model.

2. Pure plunge case

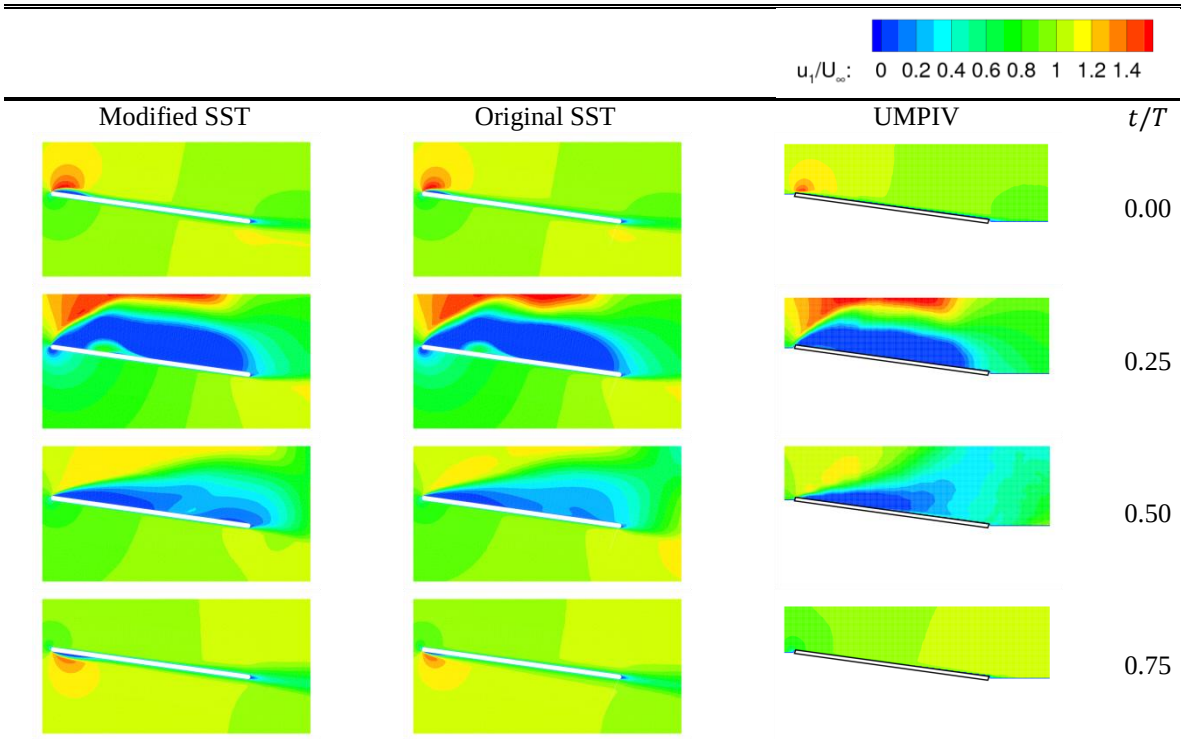

Figure 17 u_1/U_∞ contours and over pure plunging flat plate at k = 0.25, λ = 0.0, and Re = 6×10^4, k = 0.25, λ =0.0 from numerical (Modified SST, Original SST), and experimental (UM) results at t/T = 0.00, 0.25, 0.50, and 0.75.

Figure 17 shows the u_1/U_∞ contour plots from the numerical computations and the experimental measurement (UM) for the pure plunging flat plate at t/T = 0.00, 0.25, 0.50, and 0.75 at Re = 6×10^4. When the flat plate plunges down, the effective angle of attack increases to its maximum at t/T = 0.25 and generates a large vortical structure enveloping the suction side of the flat plate. This vortical structure serves as a mechanism to enhance lift by its lower pressure region in the core. The Reynolds number effect for the pure plunging case is minimal suggesting that the flow and the aerodynamic loading are either dominated by the given kinematics or the shape of the airfoil.

The u_1/U_∞ velocity profiles from two SST turbulence models agree with each other, and are close to the experimental results from the UM facility at Re = 6×10^4 for the pure plunging flat plate at different chord locations at t/T = 0.50, see Figure 18. As also the u_1/U_∞ contour plots in Figure 17 suggest the flow is characterized and the difference between the two SST models are overwhelmed by the massive separation due to the sharp leading edge, and the pure plunging kinematics with effective angles of attack exceeding the static stall values (Figure 3).

The Reynolds number effect is also minimal for the pure plunging flat plate between Re = 1×10^4 and Re = 6×10^4, as shown in Figure 19. Using the original SST turbulence model two numerical solutions at Re = 1×10^4 and Re = 6×10^4, respectively, have been computed and the resulting u_1/U_∞ velocity profiles at t/T = 0.50 show that the difference between two profiles at various chordwise locations is small.

Figure 20 shows the time history of force coefficients for the pure plunging flat plate at Re = 1×10^4, and 6×10^4 from the numerical computation using the original SST turbulence closure. The flow at Re = 3×10^4, both resulting aerodynamic forces, as well as flow structures are similar to the flow at Re = 6×10^4. Both lift and drag coefficients are negligibly affected by the Reynolds number variation. The lift coefficient reaches its maximum at t/T = 0.25, decreases, and starts to recover at t/T = 0.75. Although the maximum lift coefficient is larger than the pitching and plunging case, the mean lift/drag coefficient is smaller/larger.

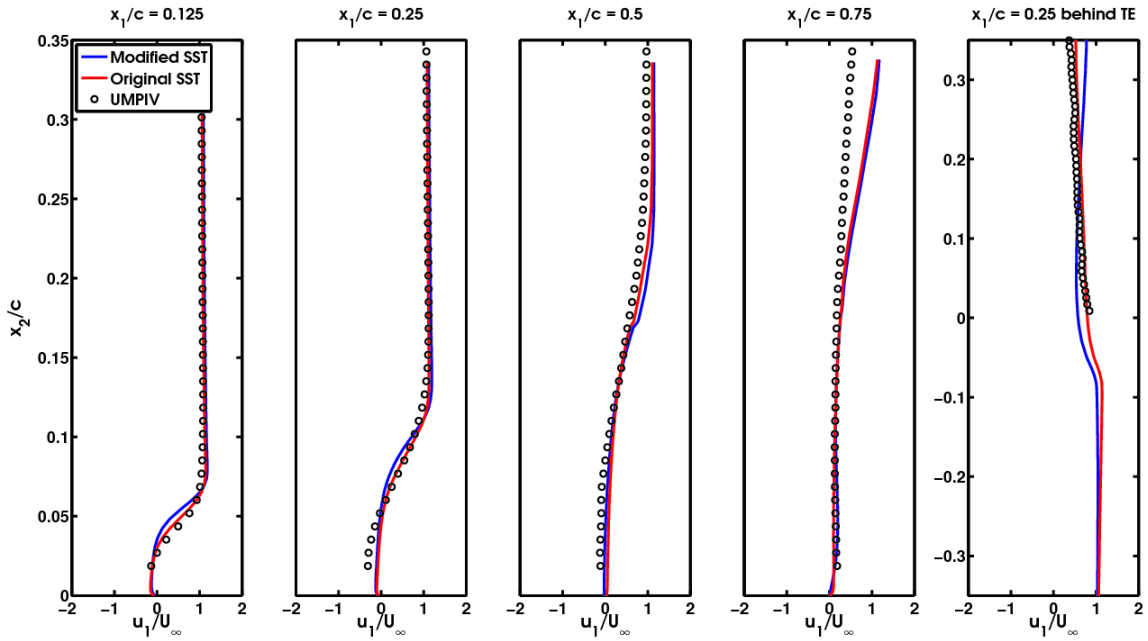

Figure 18 u_1/U_∞ profiles from the numerical (Modified SST, Original SST), and experimental (UM) results at constant x_1/c = 0.125, 0.25, 0.50, 0.75, and 0.25 behind the trailing edge at t/T = 0.50 at Re = 6×10^4, k = 0.25, λ =0.0 for the pure plunging flat plate.

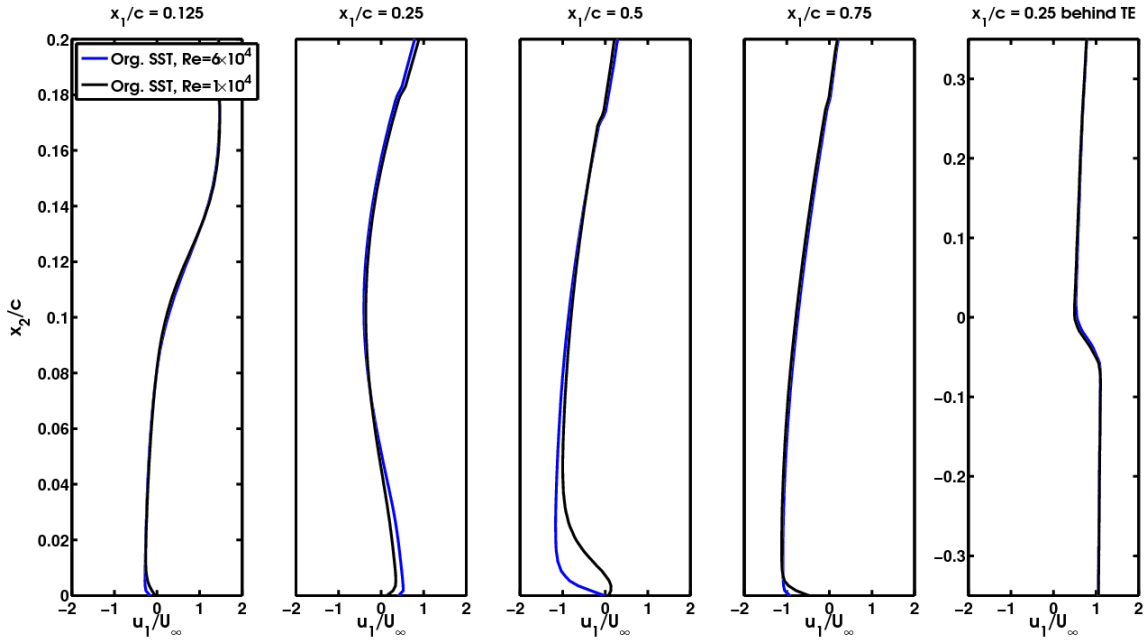

Figure 19 u_1/U_∞ profiles from the numerical (original SST) results at constant x/c = 0.125, 0.25, 0.50, 0.75, and 0.25 behind the trailing edge at t/T = 0.50 at Re = 1×10^4, and 6×10^4, k = 0.25, λ =0.0 for the pure plunging flat plate.

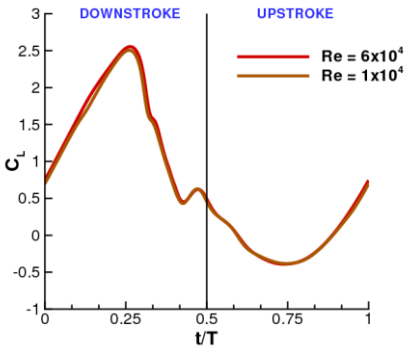

(a) lift coefficient

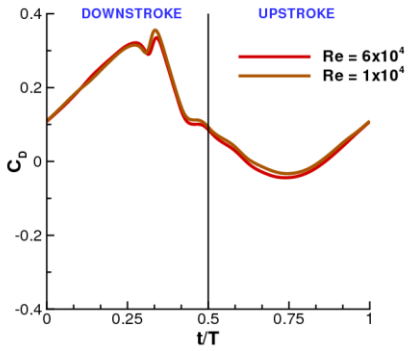

(b) drag coefficient

Figure 20. Time history of (a) lift coefficient and (b) drag coefficient for a two-dimensional flat plate at k = 0.25, and λ = 0.6 for Re = 1×10^4, and 6×10^4, respectively. Note that numerical solution is obtained using the original SST turbulence model.

D. Shape Effect on Aerodynamics: SD7003 versus Flat Plate

In order to investigate the effects of airfoil shapes in the case of pure plunging, and pitching and plunging motion on the time histories of lift coefficient, the comparisons are shown in Figure 21 for Re = 1×10^4, 6×10^4. Note that the lift coefficients are obtained using the original SST turbulence model shown in Figure 21.

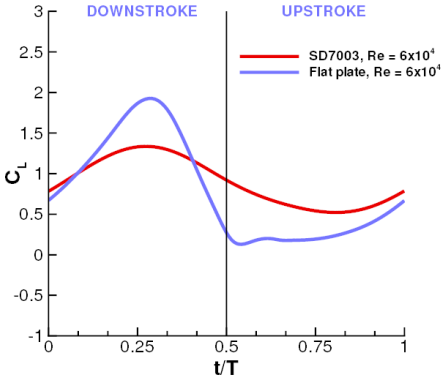

(a) pitching and plunging, Re = 6×10^4

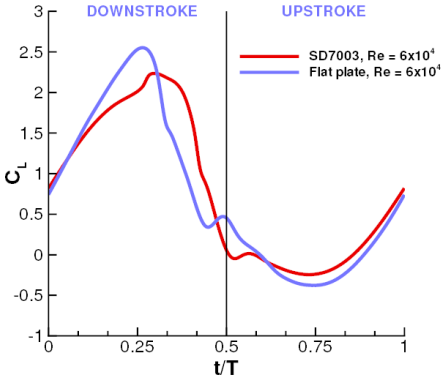

(b) pure plunging, Re = 6×10^4

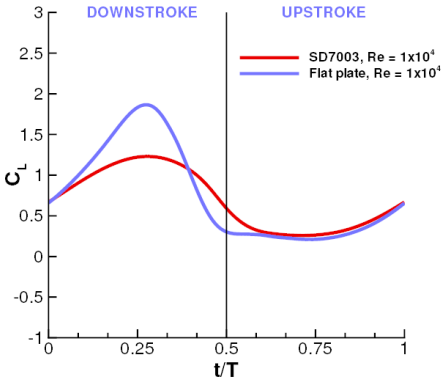

(c) pitching and plunging, Re = 1×10^4

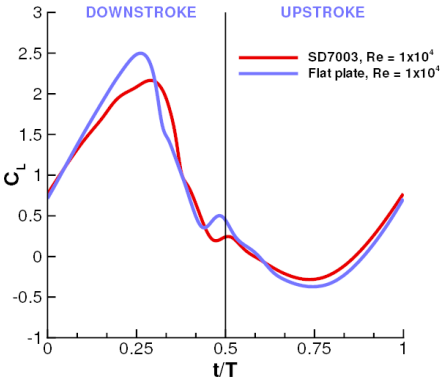

(d) pure plunging, Re = 1×10^4

Figure 21. Time histories of pitching and plunging, and pure plunging two-dimensional flat plate (blue line), and SD7003 airfoil (red line) at k = 0.25, and λ = 0.6 at Re = 1×10^4, and 6×10^4, respectively. Results using the original SST turbulence models are presented.

It is clear that the results of the flat plate (blue lines in Figure 21) showed larger lift peaks than those of the SD7003 airfoil (red lines in Figure 21) within the range of Reynolds number and airfoil kinematics considered in this study. Moreover, it is found that there is remarkable phase delay of peak in the case of pure plunging at $Re = 6\times10^4$. This is because the flow separates earlier over the flat plate during downstroke due to the sharp leading edge of the flat plate, see Figure 4, and Figure 11.

Mean and maximum force coefficients are summarized as function of Reynolds number in Appendix B (see Figure 23, and in Table 3). The maximum lift is obtained by the flat plate for both kinematics. Furthermore, the force coefficients of the flat plate are insensitive to the Reynolds number. It is also interesting to note that the mean drag coefficient is lower for the SD7003 airfoil, and the mean lift coefficient is larger for the SD7003 airfoil for $Re = 3\times10^4$, and 6×10^4

IV. Summary and Conclusion

This paper addresses modeling aspects of the fluid physics associated with two specific airfoils: a SD7003 airfoil, and a two-dimensional flat plate with 2.3% thickness undergoing two sets of wing kinematics (i.e., pitching and plunging, and pure plunging) at *Re* range from 1×10^4 to 6×10^4 and *k* of 0.25. It is found that two-dimensional RANS computations with the Menter's original and modified SST turbulence models provided qualitatively, and quantitatively - depending on the flow conditions - good predictions in terms of velocity fields compared to two-dimensional phase-averaged PIV data in the water channel from two different facilities.

Our efforts are highlighted as follows:

i) Regarding the impacts of turbulence models on flow field around the SD7003, when the flow is attached, such as under pitching and plunging motion, the original formulation of SST turbulence closure offers consistently favorable agreement with the experimental results, while the modified SST turbulence model overpredicts flow separation. This can be due to a limiter in the production term of the turbulence kinetic energy equation reducing the build-up of turbulence near stagnation point regions, reducing the eddy viscosity. On the other hand, if the flow exhibits massive separation, the modified SST turbulence model shows better prediction of the experimental results, such as capturing flow reattachment. Finally for the flat plate cases, the leading edge effects overwhelms the difference between turbulence models.

ii) For pitching and plunging case the flow over the SD7003 airfoil is attached in both experimental data, and the numerical data using the original SST turbulence model at $Re = 3\times10^4$, and 6×10^4. At $Re = 1\times10^4$ separation has been evinced from the leading edge both experimental as well as computational approaches.

iii) For pure plunging SD7003 airfoil case, depending on the turbulence characteristics including those caused the motion of the wing, and the implied eddy viscosity level, qualitatively different flow structures are observed experimentally and computationally.

iv) In case of the flow over the flat plate in all approaches the geometrical effect at the sharp leading edge of the flat plate is dominant, and triggers substantial separation from the leading edge for both kinematics.

v) Regarding the comparison between SD7003 airfoil and flat plate, we have found that the mean/max lift coefficient of the flat plate is more insensitive to the variation of Reynolds number than the SD7003 airfoil. Although the maximum lift coefficient of flat plate is larger for all Reynolds numbers considered than that of SD7003 airfoil cases, the mean lift coefficient varies more strongly with the Reynolds number. There is significant difference in instantaneous lift coefficient, and flow structures between both airfoils under the same kinematics and flow conditions.

In summary, the airfoil shape plays an important role to determine the flow features generated by the pitching and plunging, and pure plunging kinematics. Due to the larger leading edge radius of the SD7003 airfoil, the effects of Reynolds number are obviously observed. Furthermore, for pitching and plunging case, more attached flow feature are present at higher Re, whereas we observe flow separations from the leading edge observed at lower Re. For pure plunging case a leading edge separation is seen at all Reynolds numbers In addition, the discrepancies shown in the previous work[32] between the experimental and computational results at high Re that the computation could not capture the flow reattachment has been corrected by using the modified version of SST turbulence model.

Appendix

A. Spatial and Temporal Sensitivity Study

Spatial and temporal sensitivity tests for the SD7003 airfoil are performed by Kang *et al.*[32] and the solution for the pitching and plunging SD7003 airfoil with 46281 cells using T/dt = 480 is shown to be grid and time independent. In all computations the time step of T/dt = 480 have been used. For the pitching and plunging flat plate the spatial sensitivity test is investigated at Re = 6×10^4, k = 0.25, and λ = 0.6. To assess the grid sensitivity time histories of lift coefficient on the baseline (9624 cells), finer (32204 cells) and the finest (65904 cells) grids are compared in Figure 22 using a time step of T/dt = 480. All three solutions stay within maximum relative error of 2%, with the relative error between the finer and the finest grid smaller than between the baseline and the finer grid. Based on this observation, the finer grid has been chosen for all subsequent computations for the flat plate.

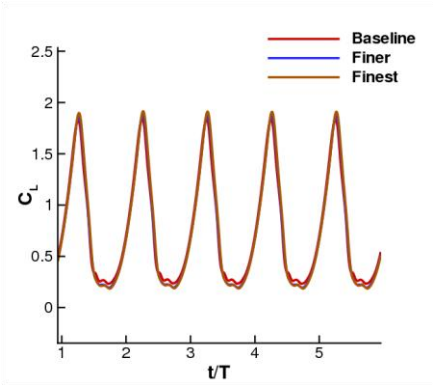

Figure 22. Time histories of the lift coefficients using the baseline (9624 cells), finer (32204 cells), and the finest (65904 cells) grid using T/dt = 480 over pitching and plunging two-dimensional flat plate at Re = 6×10^4, k = 0.25, and λ = 0.6.

B. Mean and Maximum Force Coefficient for the SD7003, and Flat Plate

Table 3 Mean and maximum lift and drag coefficients for the investigated Reynolds numbers for the SD7003 airfoil and the flat plate for the pitching and plunging, and the pure plunging at k = 0.25 using the original SST turbulence closure.

Airfoil	Kinematics	Re	$C_{L,\,mean}$	$C_{L,\,max}$	$C_{D,\,mean}$	$C_{D,\,max}$
SD7003	Pitching and Plunging	1×10^4	0.70	1.23	0.032	0.11
SD7003	Pitching and Plunging	3×10^4	0.84	1.30	0.011	0.14
SD7003	Pitching and Plunging	6×10^4	0.89	1.34	0.0039	0.15
SD7003	Pure Plunging	1×10^4	0.69	2.16	0.089	0.30
SD7003	Pure Plunging	3×10^4	0.76	2.15	0.074	0.31
SD7003	Pure Plunging	6×10^4	0.79	2.23	0.063	0.32
Flat plate	Pitching and Plunging	1×10^4	0.75	1.86	0.068	0.11
Flat plate	Pitching and Plunging	3×10^4	0.77	1.90	0.061	0.10
Flat plate	Pitching and Plunging	6×10^4	0.77	1.92	0.057	0.10
Flat plate	Pure Plunging	1×10^4	0.70	2.50	0.12	0.34
Flat plate	Pure Plunging	3×10^4	0.71	2.53	0.12	0.33
Flat plate	Pure Plunging	6×10^4	0.73	2.55	0.12	0.33

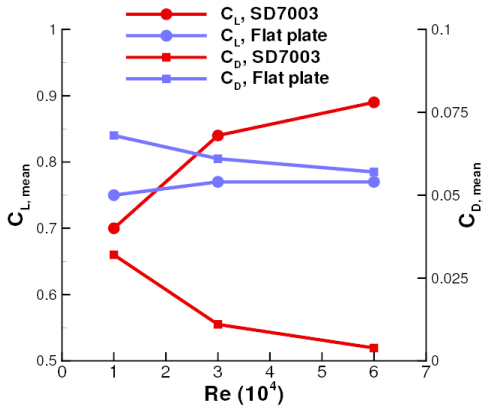

(a) pitching and plunging, mean

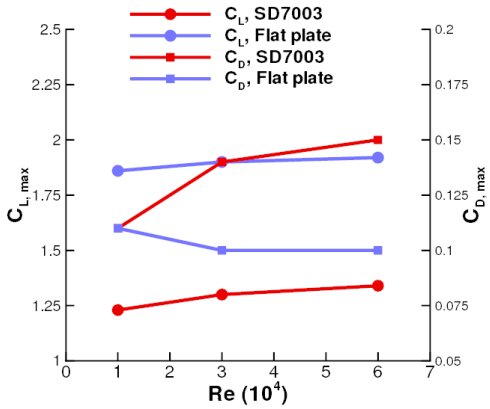

(b) pitching and plunging, max

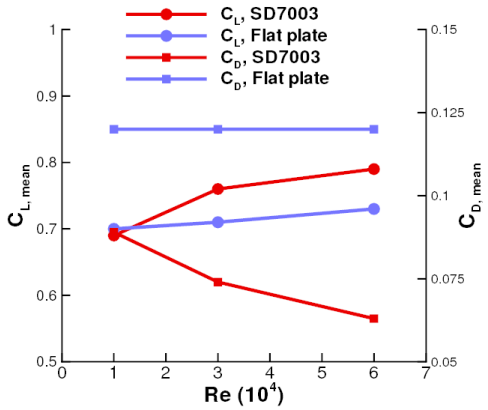

(c) Pure plunging, mean

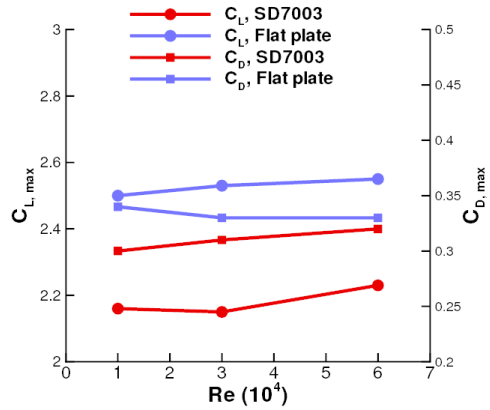

(d) Pure plunging, max

Figure 23 Mean and maximum lift and drag coefficients as function of Reynolds number for the SD7003 airfoil and the flat plate for the pitching and plunging, and the pure plunging at k = 0.25 using the original SST turbulence closure.

Acknowledgments

The work has been supported in part by the Air Force Office of Scientific Research's Multidisciplinary University Research Initiative (MURI) and by the Michigan/AFRL (Air Force Research Laboratory)/Boeing Collaborative Center in Aeronautical Sciences.

References

[1] Shyy, W., Lian, Y., Tang, J., Viieru, D., and Liu, H., *Aerodynamics of Low Reynolds Number Flyers*, Cambridge University Press, 2008

[2] Sane, P.S., and Dickinson, M.H., "The Control of Flight Force by a Flapping Wing: Lift and Drag Production," *Journal of Experimental Biology*, Vol. 204, 2001, pp. 2607–2626.

[3] Poelma, C., and Dickinson, M.H. "Time-Resolved Reconstruction of the Full Velocity Field around a Dynamically-Scaled Flapping Wing". *Experiments in Fluids*, Vol. 41, 2006, pp. 213-225

[4] Shyy, W., Trizila, P., Kang, C., and Aono, H., "Can Tip Vortices Enhance Lift of a Flapping Wing?," *AIAA J.*, Vol. 47, 2009, pp. 289-293

[5] Usherwood, J.R., and Ellington, C.P. "The Aerodynamics of Revolving Wings I. Model Hawkmoth Wings," *Journal of Experimental Biology* Vol. 205, 2002, pp. 1547–1564,

[6] Taira, K., and Colonius, T., "Three-dimensional Flows Around Low-aspect-ratio Wings at Low Reynolds Numbers," *Journal of Fluid Mechanincs*, Vol. 623, 2009, pp. 187-207

[7] Dong, H., Mittal, R., and Najjar, F.M., "Wake Topology and Hydrodynamic Performance of Low-aspect-ratio Flapping Foils," *Journal of Fluid Mechanics*, Vol. 566, 2006, pp. 309-343

[8] Taylor, G. K., Nudds, R. L., and Thomas, A. L. R., "Flying and swimming animals cruise at a Strouhal number tuned for high power efficiency", *Nature (London)* 425**,** 2003, pp. 707–711.

[9] Wang, Z.J., Birch, J., and Dickinson, M.H., "Unsteady Forces in Hovering Flight: Computation Vs. Experiments," *Journal of Experimental Biology*, Vol. 207, 2004, pp. 449–460
[10] Tang, J., Viieru, D., and Shyy, W., "Effects of Reynolds Number and Flapping Kinematics on Hovering Aerodynamics," *AIAA J.*, Vol. 46, 2008, pp. 967-976.
[11] Trizila, P., Kang, C., Visbal, M.R., and Shyy, W., "Unsteady Fluid Physics and Surrogate Modeling of Low Reynolds Number, Flapping Airfoils," AIAA Paper No. 2008-3821, 38th AIAA Fluid Dynamics Conference and Exhibit, 2008.
[12] Shyy, W., and Liu, H., "Flapping Wings and Aerodynamic Lift: The Role of Leading-Edge Vortices," *AIAA J.*, Vol. 45, 2007, pp. 2817-2819.
[13] Ramamurti, R., and Sandberg, W.C., "A Computational Investigation of the Three-Dimensional Unsteady Aerodynamics of Drosophila Hovering and Maneuvering," *Journal of Experimental Biology*, Vol. 210, 2007, pp. 881-896
[14] Aono, H., Liang, F., and Liu, H., "Near- and Far-field Aerodynamic in Insect Hovering Flight: an Integrated Computational Study," *Journal of Experimental Biology*, Vol. 211, 2008, pp. 239-257.
[15] von Karman, T., and Sears, W. R., "Airfoil Theory for Nonuniform Motion," *Journal of the Aeronautical Sciences*, Vol. 5, No. 10, 1938, pp. 379–390
[16] Koochesfahani, M.M. "Vortical Patterns in the Wake of an Oscillating Airfoil," *AIAA J.*, Vol. 27, No. 9, Sept. 1989, pp. 1200-1205.
[17] Radespiel, R., Windte, J., and Scholz, U., "Numerical and Experimental Flow Analysis of Moving Airfoils with Laminar Separation Bubbles," *AIAA J.*, Vol. 45, No. 6, 2007
[18] Windte, J., and Radespiel, R., "Propulsive Efficiency of a Moving Airfoil at Transitional Low Reynolds Numbers," *AIAA J.*, Vol. 46, No. 9, 2008
[19] McCroskey, W. J., Carr, L. W., and McAlister, K. W., "Dynamic Stall Experiments on Oscillating Airfoils," *AIAA J.*, Vol. 14, No. 1., 1976, pp. 57-63.
[20] McCroskey, W. J., "Unsteady Airfoils," *Ann. Rev. Fluid Mech.*, Vol. 14, 1982, pp. 285-311.
[21] Carr, L., "Progress in Analysis and Prediction of Dynamic Stall," *J. Aircraft*, Vol., 25, 1988, pp. 6-17.
[22] Carr, L., and McCroskey, W. J., "A Review of Recent Advances in Computational and Experimental Analysis of Dynamic Stall," *IUTAM Symp. On Fluid Dynamics of High Angle of Attack*, 1992
[23] Ohmi, K., Coutanceau, M., Loc, T. P., and Dulieu, A., "Vortex Formation around an Oscillating and Translating Airfoil at Large Incidences," *J. Fluid Mech.*, Vol. 211, 1990, pp. 37-60.
[24] Ohmi, K., Coutanceau, M., Daube, O., and Loc, T. P., "Further Experiments on Vortex Formation around an Oscillating and Translating Airfoil at Large Incidences," *J. Fluid Mech.*, Vol. 225, 1991, pp. 607-630.
[25] Visbal, M., and Shang, J. S., "Investigation of the Flow Structure Around a Rapidly Pitching Airfoil," *AIAA J.*, Vol. 27, No. 8, 1989, pp. 1044-1051.
[26] Choudhuri, G. P., and Knight, D. D., "Effects of Compressibility, Pitch Rate, and Reynolds Number on Unsteady Incipient Leading-edge Boundary Layer Separation over a Pitching Airfoil," *J. Fluid Mech.*, Vol. 308, 1996, pp. 195-217.
[27] Platzer, M., and Jones, K. "Flapping Wing Aerodynamics - Progress and Challenges" AIAA-2006-500. Jan. 2006.
[28] Young, J., and Lai, J.C.S. "Oscillation Frequency and Amplitude Effects on the Wake of a Plunging Airfoil," *AIAA Journal*, Vol. 42, No. 10, 2004. pp. 2042-2052
[29] Lian, Y., and Shyy, W., "Aerodynamics of Low Reynolds Number Plunging Airfoil under Gusty Environment," AIAA Paper 2007-71, Reno, NV, 2007.
[30] Visbal, M.R., Gordnier, R.E., and Galbraith, C., "High-fidelity Simulations of Moving and Flexible Airfoils at Low Reynolds Numbers," *Experiments in Fluids*, Vol. 46, No. 5, 2009
[31] Lentink, D., and Gerritsma, M., "Influence of Airfoil Shape on Performance in Insect Flight," AIAA-2003-3447
[32] Kang, C., Baik, Y., Bernal, L., Ol, M.V., and Shyy, W., "Fluid Dynamics of Pitching and Plunging Airfoils of Reynolds Number between 1×10^4 and 6×10^4," AIAA 2009-536
[33] Ol, M., Bernal, L., Kang, C., and Shyy, W., "Shallow and deep dynamic stall for flapping low Reynolds number airfoils," *Experiments in Fluids*, Vol. 46, Nr. 5, 2009, pp. 883-901
[34] Baik, Y., Rausch, J.M., Bernal, L.P., and Ol, M.V., "Experimental Investigation of Pitching and Plunging Airfoils at Reynolds Number between 1x10^4 and 6x10^4," AIAA 2009-4030
[35] Theodorsen, T., "General Theory of Aerodynamic Instability and the Mechanism of Flutter," *N.A.C.A. Report* 496, 1935
[36] Ol, M.V. "Vortical Structures in High Frequency Pitch and Plunge at Low Reynolds Number". AIAA-2007-4233
[37] Menter, F.R., Kuntz, M., and Langtry, R., "Ten Years of Industrial Experience with the SST Turbulence Model. In: Hanjalic, K., Nagano, Y., Tummers, M. (Eds.)," *Turbulence, Heat and Mass Transfer 4*, Begell House, 2003, pp. 625-632
[38] Menter, F.R., "Two-equation Eddy-viscosity Turbulence Models for Engineering Application," *AIAA J.*, Vol 32, 1994, pp. 269-289
[39] Kamakoti, R., Thakur, S., Wright, J., and Shyy, W., "Validation of a new parallel all-speed CFD code in a rule-based framework for multidisciplinary applications," AIAA 2006-3063

[40] Shyy, W., "A Study of Finite Difference Approximations to Steady-State, Convection-Dominated Flow Problems," *Journal of Computational Physics*, Vol. 57, No. 3, 1985, pp. 415-438.
[41] Shyy, W., *Computational Modeling for Fluid Flow and Interfacial Transport*, Elsevier, Amsterdam, 1994.
[42] Thomas, P.D., and Lombard, K., "The Geometric Conservation Law – A Link between Finite-Difference and Finite-Volume Methods of Flow Computation on Moving Grids", AIAA 1978-1208
[43] Shyy, W., Udaykumar, H.S., Rao, M.M., and Smith, R.W.,*Computational Fluid Dynamics with Moving Boundaries*, Taylor & Francis, Washington, DC, (1996, revised printing 1997, 1998 &2001); Dover, New York, 2007
[44] Sane, S.P., and Dickinson, M.H. "The Aerodynamic Effects of Wing Rotation and a Revised Quasi-Steady Model of Flapping Flight," *Journal of Experimental Biology*, Vol. 205, 2002, pp. 1087–1096.
[45] Leishman, J.G., *Principles of Helicopter Aerodynamics.*, Cambridge University Press, 2000.
[46] Anderson, .J.M., Streitlien, K., Barrett, D.S., and Triantafyllou, M.S. "Oscillating Foils of High Propulsive Efficiency," *Journal of Fluid Mechanics*, Vol. 360, 1998, pp. 41-72.
[47] Liiva, J. "Unsteady Aerodynamic and Stall Effects on Helicopter Rotor Blade Airfoil Sections". *J. Aircraft*, Vol. 6, No.1, 1969, pp. 46-51.
[48] Ol, M., McAuliffe, B. R., Hanff, E. S., Scholz, U., and Kaehler, Ch., "Comparison of Laminar Separation Bubble Measurements on a Low Reynolds Number Airfoil in Three Facilities", AIAA 2005-5149